
DiffCAP: Diffusion-based Cumulative Adversarial Purification for Vision Language Models

**Jia Fu^{1,2}, Yongtao Wu³, Yihang Chen⁴, Kunyu Peng⁵, Xiao Zhang⁶,
Volkan Cevher³, Sepideh Pashami², Anders Holst^{1,2}**

¹KTH Royal Institute of Technology ²RISE Research Institutes of Sweden

³Swiss Federal Technology Institute of Lausanne ⁴University of California, Los Angeles

⁵Karlsruhe Institute of Technology ⁶CISPA Helmholtz Center for Information Security

Abstract

Vision Language Models (VLMs) have shown remarkable capabilities in multi-modal understanding, yet their susceptibility to perturbations poses a significant threat to their reliability in real-world applications. Despite often being imperceptible to humans, these perturbations can drastically alter model outputs, leading to erroneous interpretations and decisions. This paper introduces DiffCAP, a novel diffusion-based purification strategy that can effectively neutralize adversarial corruptions in VLMs. We observe that adding minimal noise to an adversarially corrupted image significantly alters its latent embedding with respect to VLMs. Building on this insight, DiffCAP cumulatively injects random Gaussian noise into adversarially perturbed input data. This process continues until the embeddings of two consecutive noisy images reach a predefined similarity threshold, indicating a potential approach to neutralize the adversarial effect. Subsequently, a pretrained diffusion model is employed to denoise the stabilized image, recovering a clean representation suitable for the VLMs to produce an output. Through extensive experiments across six datasets with three VLMs under varying attack strengths in three task scenarios, we show that DiffCAP consistently outperforms existing defense techniques by a substantial margin. Notably, DiffCAP significantly reduces both hyperparameter tuning complexity and the required diffusion time, thereby accelerating the denoising process. Equipped with strong theoretical and empirical support, DiffCAP provides a robust and practical solution for securely deploying VLMs in adversarial environments.

Warning: This paper contains images or texts that may be considered offensive.

1 Introduction

Vision language models (VLMs) have exhibited impressive performance in a diverse range of multi-modal understanding tasks [44, 37, 23, 1], empowering numerous real-world applications such as image-grounded text generation (e.g., image captioning and visual question answering) [29, 40, 28] and zero-shot classification [44, 63, 1, 62]. However, their inherent susceptibility to adversarial perturbations presents a critical challenge [67, 43, 64]. These perturbations are usually designed to be imperceptible to humans, but when added to natural images, can deceive models into making incorrect predictions, severely undermining their reliability and effectiveness [17, 38, 8]. Adversarial vulnerability is especially concerning as malicious actors may exploit these ML systems to spread misinformation or fraudulent activities [58], highlighting the urgent need for robust defensive strategies [24, 32].

To mitigate this threat, significant research efforts have focused on adversarial defenses specifically designed for VLMs [32, 56]. A dominant direction in this field is adversarial training, which fine-tunes

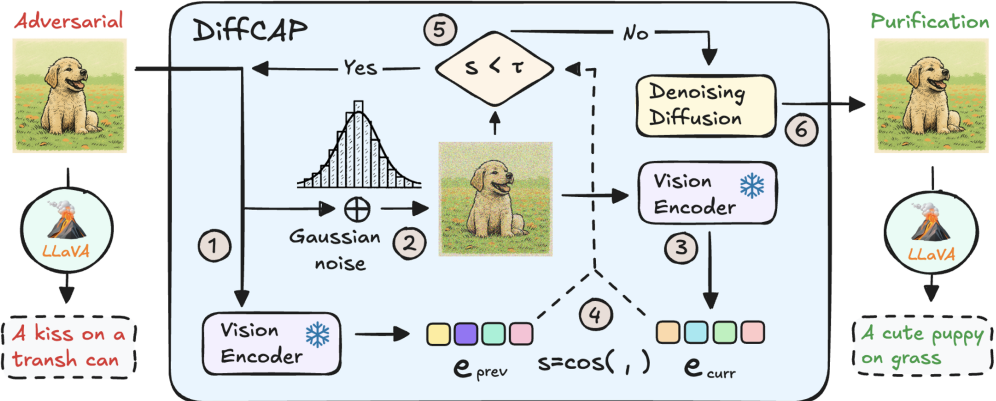


Figure 1: Overview of the DiffCAP Pipeline: An adversarial input is cumulatively processed through steps 1 to 5; if a stopping condition is not satisfied at step 5, the process restarts from step 1, otherwise the purification output is generated at step 6. See Alg. 1 for details.

models using adversarially perturbed data to enhance robustness. For instance, recent approaches such as Robust CLIP [48] have leveraged supervised adversarial fine-tuning to fortify VLMs against specific attack types. Although effective within their training scope, these methods exhibit significant limitations, particularly poor generalization to novel, unseen attacks [15, 26] and substantial computational overhead associated with continuous retraining and fine-tuning procedures [57, 2].

In contrast, adversarial purification [61, 41] emerges as a promising alternative that does not require the expensive adversarial fine-tuning of models. Techniques like DiffPure [41] have demonstrated the feasibility of purification approaches by directly removing adversarial perturbations from input data using generative models, such as diffusion models [51, 53, 60, 52]. These methods maintain a high generalization capability to unseen attacks without necessitating modifications to the underlying VLM, thus preserving original model performance on benign inputs. Despite these advantages, current generative model-based purification techniques suffer from substantial slowdown at inference time, hindering their practical deployment, particularly for real-time scenarios involving large VLMs.

To address these critical shortcomings, we propose DiffCAP, abbreviated for *Diffusion-based Cumulative Adversarial Purification*, the first adversarial purification strategy specifically designed for VLMs. DiffCAP leverages a novel mechanism that dynamically identifies the minimal necessary diffusion time, effectively balancing purification efficacy and computational efficiency. Our method cumulatively injects random Gaussian noise into adversarially perturbed images until the embeddings of two consecutively noised images converge to a predefined similarity threshold, indicating the potential neutralization of adversarial perturbations. A diffusion model subsequently denoises this stabilized image, enabling the recovery of a clean, interpretable image for VLM inference.

Contribution. The main contributions of our work can be summarized in the following aspects:

- To the best of our knowledge, DiffCAP is the first adversarial purification framework that enables fast and robust VLM inference. DiffCAP is designed to minimize the diffusion time and hyperparameter adjustments, enabling efficient training and fast inference.
- We establish a recovery region during the forward diffusion process, supported by a rigorous analysis of semantic stability in the embedding space. In particular, we prove that the semantic change between consecutive forward diffusion steps decreases as the diffusion time t grows.
- We conduct comprehensive experiments across three popular VLMs, six diverse datasets, multiple perturbation strengths, and various multimodal tasks, including image captioning, visual question answering, and zero-shot classification. The results demonstrate that DiffCAP consistently outperforms existing state-of-the-art defenses by a considerable margin.

2 Preliminaries

This section provides the background and preliminary definitions of vision encoders, including their use for both CLIP and Vision LLMs, as well as continuous-time diffusion models.

2.1 Vision encoder

CLIP. Contrastive Language-Image Pre-training (CLIP) [44] consists of a vision encoder $\phi : \mathbb{R}^d \rightarrow \mathbb{R}^m$ and a text encoder $\psi : \mathbb{R}^{d'} \rightarrow \mathbb{R}^m$. The vision encoder and the text tokenizer have the same embedding dimension. We define a zero-shot classifier h . For a K -class task, text prompts \mathbf{t}_k , such as ‘‘A photo of <class k >’’, are generated for $k = 1, \dots, K$. The classifier h , determined by ϕ and ψ , calculates logits for an input image \mathbf{x} via the cosine similarity between the image embedding and each prompt embedding:

$$h_k(\mathbf{x}) = \cos(\phi(\mathbf{x}), \psi(\mathbf{t}_k)) = \left\langle \frac{\phi(\mathbf{x})}{\|\phi(\mathbf{x})\|_2}, \frac{\psi(\mathbf{t}_k)}{\|\psi(\mathbf{t}_k)\|_2} \right\rangle. \quad (1)$$

Vision LLMs. Vision LLMs, such as LLaVA [35, 33, 36] and MiniGPT [68], consist of a vision encoder $\phi : \mathbb{R}^d \rightarrow \mathbb{R}^m$, a text tokenizer, and a language model. The vision encoder and the text tokenizer have the same embedding dimension. When feeding the VLM with an image and the instruction, a vision encoder transforms this image to hidden embeddings of dimension m . The text tokenizer first tokenizes the instruction into tokens, and then looks up the embedding matrix to get its m -dimensional embedding. The image embedding and the instruction embedding are concatenated and then fed into a language model to generate a description. The vision encoder is the vision encoder in CLIP [44], and the instruction prompt is usually like ‘‘Describe this image in detail’’.

2.2 Diffusion model

In this section, we briefly introduce the continuous-time diffusion models [53]. Let $p(\mathbf{x})$ represent the underlying, unknown distribution for data points $\mathbf{x} \in \mathbb{R}^d$. The core idea of diffusion models is to progressively transform samples from $p(\mathbf{x})$ into Gaussian noise. Formally, the transformation can be formulated by the forward diffusion process $\{\mathbf{x}(t)\}_{t \in [0,1]}$, which is governed by the following stochastic differential equation (SDE) in the time interval $[0, 1]$:

$$d\mathbf{x} = \mathbf{f}(\mathbf{x}, t)dt + g(t)d\mathbf{w}(t), \quad (2)$$

where $\mathbf{f} : \mathbb{R}^d \times \mathbb{R} \rightarrow \mathbb{R}^d$ stands for the drift function, $g : \mathbb{R} \rightarrow \mathbb{R}$ is the diffusion function, and $\mathbf{w}(t) \in \mathbb{R}^d$ denotes the Brownian motion. Note that the diffusion process starts with $\mathbf{x}(0)$ drawn from the underlying data distribution $p(\mathbf{x})$.

The distribution of $\mathbf{x}(t)$ at any time t is $p_t(\mathbf{x})$, with the initial data distribution being $p_0(\mathbf{x}) = p(\mathbf{x})$. The functions $\mathbf{f}(\mathbf{x}, t)$ and $g(t)$ are chosen carefully so that as t approaches 1, the distribution $p_1(\mathbf{x})$ closely resembles a standard d -dimensional Gaussian distribution, $\mathcal{N}(\mathbf{0}, \mathbf{I}_d)$. We follow the Variance Preserving (VP) SDE [53], where the drift and diffusion coefficients are $\mathbf{f}(\mathbf{x}, t) = -\frac{1}{2}\beta(t)\mathbf{x}$ and $g(t) = \sqrt{\beta(t)}$ respectively. Here, $\beta(t)$ is a function that controls the noise level over time.

To generate new samples, one must reverse the diffusion process. This is achieved by solving a corresponding reverse-time SDE of Eq. (2):

$$d\hat{\mathbf{x}} = [\mathbf{f}(\hat{\mathbf{x}}, t) - g(t)^2 \nabla_{\hat{\mathbf{x}}} \log p_t(\hat{\mathbf{x}})]dt + g(t)d\bar{\mathbf{w}}. \quad (3)$$

The generation process starts with drawing an initial sample $\hat{\mathbf{x}}(1)$ from the standard Gaussian distribution $\mathcal{N}(\mathbf{0}, \mathbf{I}_d)$. Then, by integrating this SDE from $t = 1$ down to $t = 0$, the noisy sample $\hat{\mathbf{x}}(t)$ is progressively denoised. The goal is for the final output $\hat{\mathbf{x}}(0)$ to be a sample from the original data distribution $p_0(\mathbf{x})$. However, the score function $\nabla_{\mathbf{x}} \log p_t(\mathbf{x})$ in Eq. (3) is usually intractable. In practice, we use a neural network, denoted by $\mathbf{s}_{\theta}(\mathbf{x}, t)$ and parameterized by θ , to approximate the score function [53, 25].

3 Related work

Perturbation-based attacks. Perturbation-based attacks cause models to make incorrect predictions by introducing small, often imperceptible, alterations to the input data [10, 22, 9]. These attacks commonly leverage gradient-based methods to find the most vulnerable parts of an input, then craft perturbations to maximize the model’s loss. A classic illustration is adversarial image attacks,

where minute pixel modifications, invisible to humans, can trick a model into misclassifying an image [17, 38].

Adversarial training. Adversarial training employs optimization techniques to bolster model robustness and safety alignment. TeCoA [39] applies supervised adversarial fine-tuning on ImageNet, while FARE [48] leverages an unsupervised adversarial fine-tuning approach using an embedding loss on PGD-perturbed [38] inputs to enhance CLIP vision encoder robustness and zero-shot performance. Addressing challenges in such methods, Hossain et al. [21] developed Sim-CLIP, which integrates a Siamese architecture with a cosine similarity loss to align clean and perturbed representations, incorporating a stop-gradient mechanism for efficient training without negative samples. This was further extended by Sim-CLIP+ [20], which tailors the cosine similarity loss and stop-gradient mechanism to defend VLMs against advanced optimization-based jailbreak attacks, preventing symmetric loss collapse while maintaining computational efficiency and robustness.

Adversarial purification. Adversarial purification techniques [49, 61] offer a distinct defense paradigm by employing generative models to sanitize images from adversarial perturbations [46, 19]. The main advantage is its “plug-in” simplicity to address new threats without the need to retrain vision models—since the adversarial images being sanitized independently of attack specifics and the vision models. However, this adaptability used to be constrained by weaker performance compared to adversarial training methods [12]. The vulnerability becomes especially clear when faced with adaptive attackers who have knowledge of the defense system [4, 54], a problem generally rooted in the inherent weaknesses of the previous generative models, such as GAN [16]. The rise of diffusion models [53], known for their generative capabilities, high sample diversity and inherent stochasticity, signals a promising direction for mitigating these persistent issues. DiffPure [41] proposed to use the diffusion model for adversarial purification. CLIPure [65] operates directly in the CLIP latent space, correcting embeddings of adversarial examples for downstream tasks. However, previous works did not discuss the optimal number of steps for forward noise-injection. DiffPure [41] and CLIPure [65] both use a fixed diffusion time, which is inflexible for different adversarial examples. We propose a threshold-based stopping criterion in our paper, and therefore reduce the number of noise-injection steps and improves performance by a significant margin.

4 Our method

In this section, we introduce DiffCAP, a purification mechanism that leverages forward diffusion dynamics and semantic stability to remove adversarial perturbations in VLMs. When we pass an adversarial image \mathbf{x}_{adv} into the diffusion model, $\mathbf{x}(t)$ follows a forward diffusion process governed by the variance-preserving stochastic differential equation:

$$d\mathbf{x}(t) = -\frac{1}{2}\beta(t)\mathbf{x}(t)dt + \sqrt{\beta(t)}d\mathbf{w}(t), \quad \mathbf{x}(0) = \mathbf{x}_{\text{adv}}, \quad (4)$$

$\beta(t) > 0$ is a smooth noise schedule, and $\mathbf{w}(t)$ is a standard Wiener process. This process has a closed-form solution at time t given by:

$$\mathbf{x}(t) = \sqrt{\alpha(t)}\mathbf{x}_{\text{adv}} + \sqrt{1 - \alpha(t)}\boldsymbol{\epsilon}, \quad \boldsymbol{\epsilon} \sim \mathcal{N}(\mathbf{0}, \mathbf{I}_d), \quad (5)$$

where $\alpha(t) = \exp\left(-\int_0^t \beta(s)ds\right)$. Our method builds upon the insight from randomized smoothing [11]: adding Gaussian noise to adversarial inputs can recover the original predictions with high probability. We need the following basic assumptions to facilitate our analysis.

Assumption 1 (Scale Invariance). *We assume that the classifier h (defined in Eq. (1)) is scale-invariant: for any scalar $\lambda > 0$ and any input $\mathbf{x} \in \mathbb{R}^d$, we have $h(\lambda\mathbf{x}) = h(\mathbf{x})$.*

Remark 1. *Asm. 1 is standard in deep learning theory and practically justified for models as we can always scale the input [66, 59].*

We now present our main result that establishes a certified recovery region under forward diffusion for the adversarial image. The proof can be found at Appx. A.1.

Theorem 1 (Certified recovery region under forward diffusion). *Let $h : \mathbb{R}^d \rightarrow [K]$ be the classifier. Let $\mathbf{x}_{\text{adv}} = \mathbf{x} + \boldsymbol{\epsilon}_{\text{adv}}$ be an adversarial example with perturbation $\boldsymbol{\epsilon}_{\text{adv}}$, and let $\mathbf{x}(t)$ be the solution to the forward diffusion process defined in Eq. (5) with a linear noise schedule $\beta(t) = \beta_{\min} + (\beta_{\max} -$*

Algorithm 1 DiffCAP: Diffusion-based Cumulative Adversarial Purification

Require: Adversarially perturbed input image \mathbf{x}_{adv} ; An image encoder $\phi(\cdot)$ (e.g., from VLM); Similarity threshold τ ; Pretrained diffusion denoiser $D(\cdot)$; Maximum number of forward diffusion steps T .

Ensure: Purified image $\mathbf{x}_{\text{clean}}$.

- 1: Initialize step counter $t \leftarrow 0$.
- 2: Set initial image $\mathbf{x}_0 \leftarrow \mathbf{x}_{\text{adv}}$.
- 3: Calculate initial embedding $\mathbf{e}_{\text{prev}} \leftarrow \phi(\mathbf{x}_0)$.
- 4: **while** $t < T$ **do** ▷ Iteratively inject noise and check stability
- 5: Inject noise into the images based on Eq. (5) to obtain $\mathbf{x}_{t+1/T}$.
- 6: Calculate current embedding $\mathbf{e}_{\text{curr}} \leftarrow \phi(\mathbf{x}_{t+1/T})$.
- 7: **if** $\cos(\mathbf{e}_{\text{curr}}, \mathbf{e}_{\text{prev}}) \geq \tau$ **then** ▷ Check if embeddings have stabilized
- 8: **break** ▷ Exit loop, stabilization reached
- 9: **end if**
- 10: Update previous embedding: $\mathbf{e}_{\text{prev}} \leftarrow \mathbf{e}_{\text{curr}}$, update $t \leftarrow t + 1/T$.
- 11: **end while**
- 12: Set the stabilized (but potentially noisy) image $\mathbf{x}_{\text{stable}} \leftarrow \mathbf{x}_t$.
- 13: Denoise the stabilized image using the diffusion model: $\mathbf{x}_{\text{clean}} \leftarrow D(\mathbf{x}_{\text{stable}})$.
- 14: **return** $\mathbf{x}_{\text{clean}}$.

$\beta_{\min})t$. Suppose there exists $\underline{p}_1, \overline{p}_2, k_1$ such that for all $t \in [0, 1]$

$$\mathbb{P}(h(\mathbf{x} + \epsilon'(t)) = k_1) \geq \underline{p}_1 > \overline{p}_2 \geq \max_{k \neq k_1} \mathbb{P}(h(\mathbf{x} + \epsilon'(t)) = k), \quad (6)$$

where $\epsilon'(t) \sim \mathcal{N}(\mathbf{0}, \frac{1-\alpha(t)}{\alpha(t)} \mathbf{I}_d)$. Define

$$t_{\min} = \frac{2M}{\sqrt{\beta_{\min}^2 + 2(\beta_{\max} - \beta_{\min})M} + \beta_{\min}}, \quad \text{where } M := \log \left(1 + \left(\frac{2\|\epsilon_{\text{adv}}\|_2}{\phi^{-1}(\underline{p}_1) - \phi^{-1}(\overline{p}_2)} \right)^2 \right).$$

Then, under Asm. 1, when $\beta_{\min} \geq M$, for all $t_{\min} \leq t \leq 1$, we have $\arg \max_{k \in [K]} \mathbb{P}(h(\mathbf{x}(t)) = k) = k_1$, i.e., the adversarial example is classified as its original label k_1 after sufficient forward diffusion.

Remark 2. Thm. 1 indicates that an adversarially perturbed image with added noise will eventually be classified correctly. Then, we can expect to use the diffusion model to remove the added noise to obtain the clean image.

Upon this point, we start to analyze the dynamics in the VLM embedding space during the forward diffusion process. In Thm. 1, we prove a certified recovery region, indicating the local smoothness of $\phi(\mathbf{x}(t))$ for $t \geq t_{\min}$. Therefore, we pose a local Lipschitz assumption after time t_{\min} :

Assumption 2. We assume ϕ is L -Lipschitz for $t \geq t_{\min}$

$$\|\phi(\mathbf{x}(t)) - \phi(\mathbf{x}(t'))\|_2 \leq L\|\mathbf{x}(t) - \mathbf{x}(t')\|_2 \quad \forall t, t' \geq t_{\min}.$$

Lemma 1. Under the same setting as in Thm. 1 and Asm. 2, let $\mathbf{x}(t)$ be defined as in Eq. (5). Then for any $t_1, t_2 \in [0, 1]$, as $t_1, t_2 \rightarrow 1$, we have: $\mathbb{E}[\|\phi(\mathbf{x}(t_1)) - \phi(\mathbf{x}(t_2))\|_2] \rightarrow 0$.

The proof is deferred to Appx. A.2. Lemma 1 shows that embeddings converge during forward diffusion, which motivates our semantic stopping criterion based on cosine similarity. We quantify this convergence rate in the following theorem:

Theorem 2. Let $\mathbf{x}(t)$ be defined as in Eq. (5). Then for small $\delta > 0$,

$$\mathbb{E}[\|\phi(\mathbf{x}(t)) - \phi(\mathbf{x}(t + \delta))\|_2] = O\left(L \cdot \delta \cdot \beta(t) \sqrt{\frac{\alpha(t)}{1 - \alpha(t)}}\right), \text{ for } t \in [t_{\min}, 1 - \delta], \quad (7)$$

where $\alpha(t) = \exp\left(-\int_0^t \beta(s) \, ds\right)$. Moreover, by using a common linear noise schedule $\beta(t) = \beta_{\min} + (\beta_{\max} - \beta_{\min})t$ with $\beta_{\min} > 0$ and $\beta_{\max} > \beta_{\min}$. Then $\beta(t) \cdot \sqrt{\frac{\alpha(t)}{1 - \alpha(t)}}$ is strictly decreasing for all $t \in [t_{\min}, 1]$.

Algorithm 2 Adaptive Similarity Threshold (τ) Calculation

Require: The dataset of clean-adversarial image pairs $D_{\text{pairs}} = \{(\mathbf{x}_{\text{clean}}, \mathbf{x}_{\text{adv}})\}$; The embedding function $\phi(\cdot)$. Maximum number of forward diffusion steps T .

Ensure: The similarity threshold τ .

- 1: Initialize step counter $t \leftarrow 0$.
- 2: **for all** pair $(\mathbf{x}_{\text{clean}}, \mathbf{x}_{\text{adv}}) \in D_{\text{pairs}}$ **do**
- 3: Set initial image $\mathbf{x}_{0, \text{clean}} \leftarrow \mathbf{x}_{\text{clean}}$, $\mathbf{x}_{0, \text{adv}} \leftarrow \mathbf{x}_{\text{adv}}$.
- 4: Calculate initial embedding $\mathbf{e}_{\text{prev, clean}} \leftarrow \phi(\mathbf{x}_{0, \text{clean}})$, $\mathbf{e}_{\text{prev, adv}} \leftarrow \phi(\mathbf{x}_{0, \text{adv}})$.
- 5: **end for**
- 6: **while** $t < 1$ **do** ▷ Iteratively inject noise and check stability
- 7: Initialize total similarity set $S_{\text{clean}} \leftarrow []$, $S_{\text{adv}} \leftarrow []$.
- 8: **for all** pair $(\mathbf{x}_{\text{clean}}, \mathbf{x}_{\text{adv}}) \in D_{\text{pairs}}$ **do**
- 9: Inject noise into the images based on Eq. (5) to obtain $\mathbf{x}_{t+1/T, \text{clean}}$, $\mathbf{x}_{t+1/T, \text{adv}}$.
- 10: Calculate current embedding $\mathbf{e}_{\text{curr, clean}} \leftarrow \phi(\mathbf{x}_{t+1/T, \text{clean}})$, $\mathbf{e}_{\text{curr, adv}} \leftarrow \phi(\mathbf{x}_{t+1/T, \text{adv}})$.
- 11: Calculate similarity $s_{\text{clean}} \leftarrow \cos(\mathbf{e}_{\text{curr, clean}}, \mathbf{e}_{\text{prev, clean}})$, $s_{\text{adv}} \leftarrow \cos(\mathbf{e}_{\text{curr, adv}}, \mathbf{e}_{\text{prev, adv}})$.
- 12: Add the similarity score to the set $S_{\text{clean}} \leftarrow S_{\text{clean}} \cup \{s_{\text{clean}}\}$, $S_{\text{adv}} \leftarrow S_{\text{adv}} \cup \{s_{\text{adv}}\}$.
- 13: **end for**
- 14: **if** S_{adv} and S_{clean} are from the same underlying distribution **then**
- 15: **break**
- 16: **end if**
- 17: **for all** pair $(\mathbf{x}_{\text{clean}}, \mathbf{x}_{\text{adv}}) \in D_{\text{pairs}}$ **do**
- 18: Update previous embedding: $\mathbf{e}_{\text{prev, clean}} \leftarrow \mathbf{e}_{\text{curr, clean}}$, $\mathbf{e}_{\text{prev, adv}} \leftarrow \mathbf{e}_{\text{curr, adv}}$.
- 19: **end for**
- 20: Update $t \leftarrow t + 1/T$.
- 21: **end while**
- 22: **return** $\tau \leftarrow \text{mean}(S_{\text{clean}})$.

The proof is deferred to Appx. A.3. Thm. 2 quantifies the semantic change between adjacent forward diffusion steps. The bound in Eq. (7) decreases as $t \rightarrow 1$ under the common linear noise schedule. Consequently, the expected semantic change between adjacent forward diffusion steps diminishes as the process approaches terminal time.

Our results suggest a simple yet powerful strategy: inject Gaussian noise until the semantic embedding stabilizes. We call this algorithm DiffCAP, summarized in Alg. 1. The cumulative diffusion continues until the cosine similarity between consecutive embeddings exceeds a threshold τ . A pretrained diffusion model is then applied in reverse to recover a clean image from the stabilized noisy input.

In Alg. 2, we describe how to select the threshold τ . The core idea is to iteratively inject noise into both clean and adversarial images and track the cosine similarity between the embeddings of one clean or adversarial image after two consecutive steps of noise injection. This is done for a collection of image pairs to reduce randomness. The process continues until the set of similarity scores for adversarial images and the set for clean images are statistically indistinguishable (i.e., likely from the same underlying distribution). At this point, the algorithm determines that the noise has reached a level where the embeddings' stability is comparable for both types of images.

5 Experiments

5.1 Settings

Models, datasets & metrics. We evaluate DiffCAP across three vision-language tasks: image captioning (IC), visual question answering (VQA), and zero-shot classification (ZSC). For IC and VQA, we adopt two large VLMs—OpenFlamingo (OF) [6] with 9B parameters and LLaVA-1.5 [34] with 7B parameters. For ZSC, we utilize CLIP [44] with 88M parameters as the backbone model. Our experiments are conducted on standard benchmarks: COCO [31] and Flickr30k [42] for IC, VQAv2 [18] and TextVQA [50] for VQA, and CalTech101 [27] and ImageNet1K [13] for ZSC. For both adversarial and clean evaluation, we randomly sample 500 images for IC and VQA, while 1,000

Table 1: CIDEr score of two VLMs in IC task on two datasets with clean images and adversarial perturbations of two sizes under different defenses. 2 and 4 with TeCoA and FARE suggest the version that is fine-tuned by $\ell_\infty^{2/255}$ and $\ell_\infty^{4/255}$ bounded adversarial examples, respectively. The best result is in **bold** and the runner-up is underlined.

Defense	OF-9B [6]						LLaVA 1.5-7B [34]					
	COCO [31]			Flickr30k [42]			COCO [31]			Flickr30k [42]		
	clean	$\ell_\infty^{2/255}$	$\ell_\infty^{4/255}$	clean	$\ell_\infty^{2/255}$	$\ell_\infty^{4/255}$	clean	$\ell_\infty^{2/255}$	$\ell_\infty^{4/255}$	clean	$\ell_\infty^{2/255}$	$\ell_\infty^{4/255}$
No defense	79.7	1.5	1.1	60.1	0.7	0.4	115.5	4.0	3.1	77.5	1.6	1.0
TeCoA ² [39]	73.5	<u>31.6</u>	21.2	49.5	<u>14.1</u>	9.5	98.4	<u>44.2</u>	30.3	57.1	<u>23.2</u>	15.3
FARE ² [48]	79.1	34.2	19.5	57.7	16.4	8.9	109.9	53.6	31.0	71.1	29.5	17.5
TeCoA ⁴ [39]	66.9	28.5	21.6	40.9	12.0	10.3	88.3	50.9	35.3	48.6	27.9	19.5
FARE ⁴ [48]	74.1	30.9	22.8	51.4	15.7	10.5	102.4	<u>57.1</u>	40.9	61.6	<u>31.4</u>	22.8
JPEG-DL [45]	78.2	<u>66.1</u>	43.9	<u>58.8</u>	<u>47.6</u>	30.7	113.3	<u>106.4</u>	<u>77.2</u>	74.8	<u>69.6</u>	47.9
DiffPure [41]	74.9	<u>73.4</u>	<u>72.3</u>	49.8	<u>49.2</u>	<u>50.3</u>	106.5	<u>108.4</u>	<u>105.0</u>	65.5	66.4	<u>63.2</u>
CLIPure [65]	<u>80.8</u>	6.6	5.3	59.3	4.7	3.5	<u>115.1</u>	4.9	3.4	76.9	2.1	1.5
DiffCAP	81.4	79.3	78.4	55.6	56.7	57.2	120.4	119.6	116.9	75.0	72.7	72.1

images are chosen for ZSC. We report Consensus-based Image Description Evaluation (CIDEr) [55] score for IC, VQA accuracy [3] for VQA, and top-1 accuracy for ZSC.

Attacks. The attack is conducted in the *gray-box* setting, where the adversary can access the gradients of the model but has no knowledge of the defense pipeline. For IC and VQA, we adopt a two-stage attack pipeline following [47]. In the first stage, we apply 100-step Auto-PGD (APGD) attacks [12] in half-precision using multiple ground-truth captions or answers as supervision. Samples that fall below a predefined performance threshold are excluded from further attacks. In the second stage, we conduct stronger single-precision APGD attacks on the remaining samples. This progressive strategy maximizes adversarial impact while remaining computationally efficient. For ZSC, we follow the AutoAttack framework, employing APGD with cross-entropy loss and targeted Difference of Logits Ratio (DLR) loss with 100 iterations, respectively.

Baselines. We compare DiffCAP with two categories of adversarial defense methods. The first category includes adversarially fine-tuned vision encoders. Since both OF and LLaVA adopt CLIP as their vision backbone, we replace their CLIP vision encoder with two robust variants: TeCoA [39] and FARE [48]. TeCoA applies supervised adversarial training, while FARE employs an unsupervised loss. The second category includes purification methods. We consider: JPEG-DL [45], the trainable JPEG compression layer to remove adversarial perturbations; DiffPure [41], the first approach leveraging the diffusion process to recover the clean image in the pixel space; CLIPure [65], the latest method that operates directly in the CLIP latent space.

Hyperparameters. The algorithms are implemented through PyTorch, and all experiments are conducted on an NVIDIA A100 GPU. By default, we use the ViT-B/32 CLIP vision encoder to ensure computational efficiency. We take advantage of the pre-trained diffusion model from [14]. Following Alg. 2, we determine the threshold $\tau = 0.96$ on subsets comprising 100 random images from each of the datasets mentioned above. For all the experiments, we fix the threshold. More experimental details can be found in the supplementary material.

5.2 Result analysis

Image captioning. As shown in Tab. 1, VLMs are highly vulnerable to adversarial perturbations: even 2/255 attacks can reduce CIDEr scores close to zero. Adversarial training methods (TeCoA and FARE) provide moderate robustness improvements. However, their effectiveness drops significantly under 4/255 attacks. Notably, TeCoA and FARE also degrade the clean performance, especially on Flickr30k. JPEG-DL shows better robustness than TeCoA and FARE, but remains sensitive to perturbation strength. DiffPure substantially improves robustness, lifting performance under both 2/255 and 4/255 attacks to levels comparable with clean conditions. DiffCAP consistently outperforms all baselines across both models and datasets. It achieves significantly better robustness than DiffPure under both attack strengths, and requires less than 1/3 of DiffPure’s denoising runtime

Table 2: Accuracy (%) of two VLMs in VQA task on two datasets with clean images and adversarial perturbations of two sizes under different defenses. 2 and 4 with TeCoA and FARE suggest the version that is fine-tuned by ℓ_∞ -norm bounded adversarial examples with $\epsilon = 2/255$ and with $\epsilon = 4/255$, respectively. The best result is in **bold** and the runner-up is underlined.

Defense	OF-9B [6]						LLaVA 1.5-7B [34]					
	TextVQA [50]			VQAv2 [18]			TextVQA [50]			VQAv2 [18]		
	clean	$\ell_\infty^{2/255}$	$\ell_\infty^{4/255}$	clean	$\ell_\infty^{2/255}$	$\ell_\infty^{4/255}$	clean	$\ell_\infty^{2/255}$	$\ell_\infty^{4/255}$	clean	$\ell_\infty^{2/255}$	$\ell_\infty^{4/255}$
No defense	23.8	0.0	0.0	48.5	1.8	0.0	37.1	0.5	0.0	74.5	2.9	0.0
TeCoA ² [39]	16.6	3.5	2.1	46.2	23.5	20.5	24.1	12.1	8.8	66.9	33.8	21.8
FARE ² [48]	<u>21.6</u>	4.1	1.9	<u>47.0</u>	24.0	17.2	31.9	14.7	9.1	<u>71.7</u>	34.9	23.0
TeCoA ⁴ [39]	15.4	2.1	1.8	44.8	23.6	21.3	20.7	12.6	9.3	63.2	41.0	31.7
FARE ⁴ [48]	18.6	3.4	2.9	46.1	23.6	21.0	27.6	15.8	10.9	68.3	40.7	30.5
JPEG-DL [45]	23.4	<u>15.9</u>	13.1	46.8	39.5	32.4	<u>34.6</u>	<u>27.2</u>	21.1	68.8	60.8	45.8
DiffPure [41]	13.6	13.2	<u>13.5</u>	45.1	<u>43.5</u>	<u>43.6</u>	20.9	22.0	<u>22.2</u>	67.3	<u>65.8</u>	<u>66.0</u>
CLIPure [65]	20.5	6.8	8.8	47.3	18.8	17.5	36.1	2.1	1.4	73.3	4.6	2.1
DiffCAP	18.6	16.2	16.7	46.3	45.4	45.3	28.3	29.0	28.9	70.3	69.1	68.5

Table 3: Top-1 accuracy (%) of CLIP in ZSC task with clean images and adversarial perturbations of two sizes under different defenses. 2 and 4 with TeCoA and FARE suggest the version that is fine-tuned by ℓ_∞ -norm bounded adversarial examples, respectively. The best result is in **bold** and the runner-up is underlined.

Defense	CalTech101 [27]			ImageNet1K [13]		
	clean $\ell_\infty^{2/255}$ $\ell_\infty^{4/255}$			clean $\ell_\infty^{2/255}$ $\ell_\infty^{4/255}$		
	clean	$\ell_\infty^{2/255}$	$\ell_\infty^{4/255}$	clean	$\ell_\infty^{2/255}$	$\ell_\infty^{4/255}$
No defense	83.3	0.0	0.0	87.9	0.0	0.0
TeCoA ² [39]	80.7	<u>70.2</u>	57.4	80.1	<u>58.8</u>	36.7
FARE ² [48]	84.8	73.0	46.6	85.5	56.5	25.6
TeCoA ⁴ [39]	78.4	69.7	60.9	74.3	59.2	41.9
FARE ⁴ [48]	84.7	76.7	64.1	80.2	61.6	40.6
JPEG-DL [45]	83.9	<u>68.5</u>	33.4	87.8	48.5	16.4
DiffPure [41]	83.6	83.2	83.1	81.0	79.7	79.7
CLIPure [65]	82.9	80.8	80.1	87.7	85.4	84.6
DiffCAP	82.6	<u>81.7</u>	80.9	87.2	84.4	81.1

Table 4: Top-1 accuracy (%) in ZSC task with clean images and adversarial perturbations. We use different CLIP vision encoders for DiffCAP. Numbers in parentheses denote parameters in M.

Encoder				
	clean	$\ell_\infty^{2/255}$	$\ell_\infty^{4/255}$	
CaTech [27]	RN50 (102)	82.8	82.2	82.5
	RN101 (123)	83.2	83.1	81.2
	ViT-B/32 (88)	82.6	81.7	80.9
	ViT-B/16 (149)	83.0	82.3	80.9
	ViT-L/14 (304)	82.1	82.4	81.5
ImageNet [13]	RN50 (102)	84.2	82.9	80.8
	RN101 (123)	86.7	85.5	84.1
	ViT-B/32 (88)	87.2	84.4	81.1
	ViT-B/16 (149)	84.7	85.0	82.2
	ViT-L/14 (304)	85.5	83.2	81.4

(suggested by Fig. 2). For instance, DiffCAP improves CIDEr scores by over 10% with OF on Flickr30k and with LLaVA on COCO compared to DiffPure. Furthermore, DiffCAP maintains or even improves clean performance, demonstrating strong fidelity preservation. Lastly, CLIPure performs poorly in this task. Its limited effectiveness likely stems from token-level misalignment: purifying only the [CLS] token embedding fails to influence generation-related latent tokens, which dominate the captioning process.

Visual question answering. The results in Tab. 2 mirror the trends observed in Tab. 1. DiffCAP consistently delivers the strongest performance across all attack settings compared to all baselines in both datasets and models. The improvement is particularly notable with LLaVA on TextVQA, where DiffCAP surpasses DiffPure by over 30%. Remarkably, on the TextVQA dataset, DiffPure performs worse than JPEG-DL, indicating that visual reasoning tasks depend more heavily on fine-grained visual features, which are susceptible to over-smoothing or distortion during purification. This underscores the importance of preserving semantic fidelity when applying generative models for purification. DiffCAP addresses this by dynamically calculating the minimal diffusion time required to remove adversarial noise for each individual image, thereby achieving a better trade-off between robustness and feature integrity for multi-hop reasoning tasks.

Zero-shot classification. From Tab. 3, we observe that JPEG-DL underperforms compared to TeCoA and FARE, particularly under stronger attacks. CLIPure recovers its defense effectiveness, as only the [CLS] token is involved in prediction and no generative decoding is required. On CalTech101, DiffCAP outperforms CLIPure under attacks, and on ImageNet1K, DiffCAP achieves

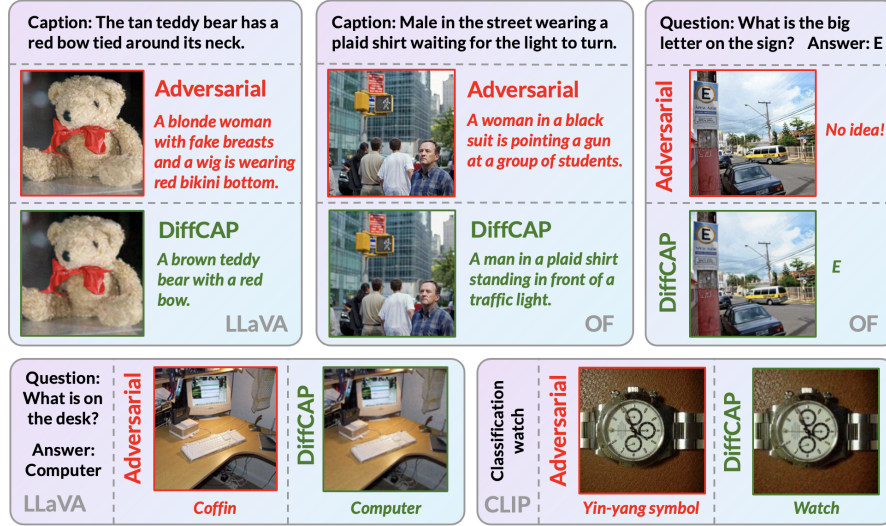


Figure 3: Adversarial examples and their DiffCAP purified counterparts under different tasks. Ground-truth labels are shown in black text.

higher robustness than DiffPure. These results confirm the generalizability of DiffCAP: it not only excels in complex vision-language tasks requiring rich semantics but also delivers stable performance on standard classification benchmarks with more sparse semantic demands.

Fig. 3 showcases the purification outcome of DiffCAP in IC, VQA, and ZSC scenarios. As a generative adversarial purification method, it introduces no noticeable degradation in fidelity. DiffCAP prominently mitigates the tension between robustness, efficiency, and image quality, establishing a new state-of-the-art among both purification- and training-based defenses for VLMs.

Ablation study and adaptive attack. We conduct systematic ablation studies to validate the utility of DiffCAP. Tab. 4 presents results obtained by replacing the vision encoder in DiffCAP with different CLIP backbones. The results illustrate that DiffCAP is largely insensitive to the choice of vision encoder, maintaining robustness across all variants. Further ablations on the diffusion step size and threshold selection are provided in the supplementary material. We also analyze the performance of DiffCAP under adaptive attacks where the adversary simulates randomness [5] and gradient obfuscation [4], with results and discussions supplemented.

6 Conclusion

In conclusion, this paper proposes DiffCAP, an efficient and theoretically inspired defense strategy for VLMs, supported by a certified recovery region under forward diffusion. By leveraging cumulative Gaussian noise injection and a semantic similarity-based stopping criterion, DiffCAP dynamically identifies the minimal purification steps required before denoising, substantially reducing computational overhead while maintaining high fidelity. DiffCAP consistently outperforms existing defenses across diverse tasks, models, and datasets, as demonstrated in extensive experiments.

Limitations. While our method is highly effective in the vision modality, an important limitation is its current reliance on image-based diffusion models. Extending the cumulative purification framework to text or multimodal diffusion processes remains an open direction, potentially broadening its applicability to text attack or joint vision-text adversarial threats.

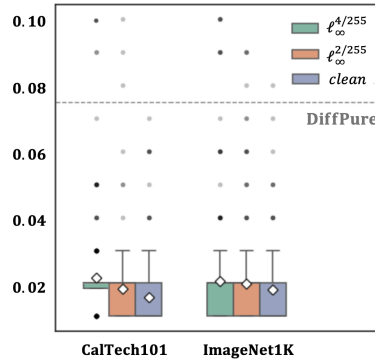


Figure 2: The box plot of DiffCAP’s diffusion time t (y -axis) before existing noise injection loop. The dashline ($t = 0.075$) is DiffPure’s noise injection time. DiffCAP requires significantly smaller diffusion time than DiffPure. The dots mark outliers and rhombuses mark mean values.

Acknowledgement

This work was financially supported by the Swedish Wireless Innovation Network (SweWIN) approved by the Swedish Innovation Agency (VINNOVA). The computations were enabled by the resources provided by the National Academic Infrastructure for Supercomputing in Sweden (NAIIS), partially funded by the Swedish Research Council. This work was also supported by the Swiss National Science Foundation (SNSF) under grant number 200021_205011. Research was sponsored by the Army Research Office and was accomplished under Grant Number W911NF-24-1-0048. This work was supported by Hasler Foundation Program: Hasler Responsible AI (project number 21043).

References

- [1] Jean-Baptiste Alayrac, Jeff Donahue, Pauline Luc, Antoine Miech, Iain Barr, Yana Hasson, Karel Lenc, Arthur Mensch, Katherine Millican, Malcolm Reynolds, et al. Flamingo: a visual language model for few-shot learning. *Advances in neural information processing systems*, 35:23716–23736, 2022.
- [2] Maksym Andriushchenko and Nicolas Flammarion. Understanding and improving fast adversarial training. *Advances in Neural Information Processing Systems*, 33:16048–16059, 2020.
- [3] Stanislaw Antol, Aishwarya Agrawal, Jiasen Lu, Margaret Mitchell, Dhruv Batra, C Lawrence Zitnick, and Devi Parikh. Vqa: Visual question answering. In *Proceedings of the IEEE international conference on computer vision*, pages 2425–2433, 2015.
- [4] Anish Athalye, Nicholas Carlini, and David Wagner. Obfuscated gradients give a false sense of security: Circumventing defenses to adversarial examples. In *International conference on machine learning*, pages 274–283. PMLR, 2018.
- [5] Anish Athalye, Logan Engstrom, Andrew Ilyas, and Kevin Kwok. Synthesizing robust adversarial examples. In *International conference on machine learning*, pages 284–293. PMLR, 2018.
- [6] Anas Awadalla, Irena Gao, Josh Gardner, Jack Hessel, Yusuf Hanafy, Wanrong Zhu, Kalyani Marathe, Yonatan Bitton, Samir Gadre, Shiori Sagawa, et al. Openflamingo: An open-source framework for training large autoregressive vision-language models. *arXiv preprint arXiv:2308.01390*, 2023.
- [7] Nicholas Carlini, Milad Nasr, Christopher A Choquette-Choo, Matthew Jagielski, Irena Gao, Pang Wei W Koh, Daphne Ippolito, Florian Tramer, and Ludwig Schmidt. Are aligned neural networks adversarially aligned? *Advances in Neural Information Processing Systems*, 36, 2024.
- [8] Nicholas Carlini and David Wagner. Towards evaluating the robustness of neural networks. In *2017 ieee symposium on security and privacy (sp)*, pages 39–57. Ieee, 2017.
- [9] Anirban Chakraborty, Manaar Alam, Vishal Dey, Anupam Chattopadhyay, and Debdeep Mukhopadhyay. Adversarial attacks and defences: A survey. *arXiv preprint arXiv:1810.00069*, 2018.
- [10] Anirban Chakraborty, Manaar Alam, Vishal Dey, Anupam Chattopadhyay, and Debdeep Mukhopadhyay. A survey on adversarial attacks and defences. *CAAI TIT*, pages 25–45, 2021.
- [11] Jeremy Cohen, Elan Rosenfeld, and Zico Kolter. Certified adversarial robustness via randomized smoothing. In *international conference on machine learning*, pages 1310–1320. PMLR, 2019.
- [12] Francesco Croce and Matthias Hein. Reliable evaluation of adversarial robustness with an ensemble of diverse parameter-free attacks. In *International conference on machine learning*, pages 2206–2216. PMLR, 2020.
- [13] Jia Deng, Wei Dong, Richard Socher, Li-Jia Li, Kai Li, and Li Fei-Fei. Imagenet: A large-scale hierarchical image database. In *2009 IEEE conference on computer vision and pattern recognition*, pages 248–255. Ieee, 2009.

[14] Prafulla Dhariwal and Alexander Nichol. Diffusion models beat gans on image synthesis. *Advances in neural information processing systems*, 34:8780–8794, 2021.

[15] Hadi M Dolatabadi, Sarah Erfani, and Christopher Leckie. ℓ_∞ -robustness and beyond: Unleashing efficient adversarial training. In *European Conference on Computer Vision*, pages 467–483. Springer, 2022.

[16] Ian Goodfellow, Jean Pouget-Abadie, Mehdi Mirza, Bing Xu, David Warde-Farley, Sherjil Ozair, Aaron Courville, and Yoshua Bengio. Generative adversarial networks. *Communications of the ACM*, 63(11):139–144, 2020.

[17] Ian J Goodfellow, Jonathon Shlens, and Christian Szegedy. Explaining and harnessing adversarial examples. *arXiv preprint arXiv:1412.6572*, 2014.

[18] Yash Goyal, Tejas Khot, Douglas Summers-Stay, Dhruv Batra, and Devi Parikh. Making the v in vqa matter: Elevating the role of image understanding in visual question answering. In *Proceedings of the IEEE conference on computer vision and pattern recognition*, pages 6904–6913, 2017.

[19] Mitch Hill, Jonathan Craig Mitchell, and Song-Chun Zhu. Stochastic security: Adversarial defense using long-run dynamics of energy-based models. In *International Conference on Learning Representations*, 2021.

[20] Md Zarif Hossain and Ahmed Imteaj. Securing vision-language models with a robust encoder against jailbreak and adversarial attacks. *arXiv preprint arXiv:2409.07353*, 2024.

[21] Md Zarif Hossain and Ahmed Imteaj. Sim-clip: Unsupervised siamese adversarial fine-tuning for robust and semantically-rich vision-language models. *arXiv preprint arXiv:2407.14971*, 2024.

[22] Sandy Huang, Nicolas Papernot, Ian Goodfellow, Yan Duan, and Pieter Abbeel. Adversarial attacks on neural network policies. *arXiv preprint arXiv:1702.02284*, 2017.

[23] Chao Jia, Yinfei Yang, Ye Xia, Yi-Ting Chen, Zarana Parekh, Hieu Pham, Quoc Le, Yun-Hsuan Sung, Zhen Li, and Tom Duerig. Scaling up visual and vision-language representation learning with noisy text supervision. In *International conference on machine learning*, pages 4904–4916. PMLR, 2021.

[24] Haibo Jin, Leyang Hu, Xinuo Li, Peiyan Zhang, Chonghan Chen, Jun Zhuang, and Haohan Wang. Jailbreakzoo: Survey, landscapes, and horizons in jailbreaking large language and vision-language models. *arXiv preprint arXiv:2407.01599*, 2024.

[25] Diederik Kingma, Tim Salimans, Ben Poole, and Jonathan Ho. Variational diffusion models. *Advances in neural information processing systems*, 34:21696–21707, 2021.

[26] Cassidy Laidlaw, Sahil Singla, and Soheil Feizi. Perceptual adversarial robustness: Defense against unseen threat models. *arXiv preprint arXiv:2006.12655*, 2020.

[27] Fei-Fei Li, Marco Andreetto, Marc’Aurelio Ranzato, and Pietro Perona. Caltech 101, Apr 2022.

[28] Junnan Li, Dongxu Li, Caiming Xiong, and Steven Hoi. Blip: Bootstrapping language-image pre-training for unified vision-language understanding and generation. In *International conference on machine learning*, pages 12888–12900. PMLR, 2022.

[29] Xiujun Li, Xi Yin, Chunyuan Li, Pengchuan Zhang, Xiaowei Hu, Lei Zhang, Lijuan Wang, Houdong Hu, Li Dong, Furu Wei, et al. Oscar: Object-semantics aligned pre-training for vision-language tasks. In *Computer Vision–ECCV 2020: 16th European Conference, Glasgow, UK, August 23–28, 2020, Proceedings, Part XXX 16*, pages 121–137. Springer, 2020.

[30] Yifan Li, Yifan Du, Kun Zhou, Jinpeng Wang, Wayne Xin Zhao, and Ji-Rong Wen. Evaluating object hallucination in large vision-language models. *arXiv preprint arXiv:2305.10355*, 2023.

[31] Tsung-Yi Lin, Michael Maire, Serge Belongie, James Hays, Pietro Perona, Deva Ramanan, Piotr Dollár, and C Lawrence Zitnick. Microsoft coco: Common objects in context. In *Computer Vision–ECCV 2014: 13th European Conference, Zurich, Switzerland, September 6–12, 2014, Proceedings, Part V 13*, pages 740–755. Springer, 2014.

[32] Daizong Liu, Mingyu Yang, Xiaoye Qu, Pan Zhou, Yu Cheng, and Wei Hu. A survey of attacks on large vision-language models: Resources, advances, and future trends. *arXiv preprint arXiv:2407.07403*, 2024.

[33] Haotian Liu, Chunyuan Li, Yuheng Li, and Yong Jae Lee. Improved baselines with visual instruction tuning, 2023.

[34] Haotian Liu, Chunyuan Li, Yuheng Li, and Yong Jae Lee. Improved baselines with visual instruction tuning. In *Proceedings of the IEEE/CVF Conference on Computer Vision and Pattern Recognition*, pages 26296–26306, 2024.

[35] Haotian Liu, Chunyuan Li, Yuheng Li, Bo Li, Yuanhan Zhang, Sheng Shen, and Yong Jae Lee. Llava-next: Improved reasoning, ocr, and world knowledge, January 2024.

[36] Haotian Liu, Chunyuan Li, Qingyang Wu, and Yong Jae Lee. Visual instruction tuning, 2023.

[37] Jiasen Lu, Dhruv Batra, Devi Parikh, and Stefan Lee. Vilbert: Pretraining task-agnostic visiolinguistic representations for vision-and-language tasks. *Advances in neural information processing systems*, 32, 2019.

[38] Aleksander Madry, Aleksandar Makelov, Ludwig Schmidt, Dimitris Tsipras, and Adrian Vladu. Towards deep learning models resistant to adversarial attacks. *arXiv preprint arXiv:1706.06083*, 2017.

[39] Chengzhi Mao, Scott Geng, Junfeng Yang, Xin Wang, and Carl Vondrick. Understanding zero-shot adversarial robustness for large-scale models. *arXiv preprint arXiv:2212.07016*, 2022.

[40] Ron Mokady, Amir Hertz, and Amit H Bermano. Clipcap: Clip prefix for image captioning. *arXiv preprint arXiv:2111.09734*, 2021.

[41] Weili Nie, Brandon Guo, Yujia Huang, Chaowei Xiao, Arash Vahdat, and Anima Anandkumar. Diffusion models for adversarial purification. *arXiv preprint arXiv:2205.07460*, 2022.

[42] Bryan A Plummer, Liwei Wang, Chris M Cervantes, Juan C Caicedo, Julia Hockenmaier, and Svetlana Lazebnik. Flickr30k entities: Collecting region-to-phrase correspondences for richer image-to-sentence models. In *Proceedings of the IEEE international conference on computer vision*, pages 2641–2649, 2015.

[43] Xiangyu Qi, Kaixuan Huang, Ashwinee Panda, Peter Henderson, Mengdi Wang, and Prateek Mittal. Visual adversarial examples jailbreak aligned large language models. In *Proceedings of the AAAI conference on artificial intelligence*, volume 38, pages 21527–21536, 2024.

[44] Alec Radford, Jong Wook Kim, Chris Hallacy, Aditya Ramesh, Gabriel Goh, Sandhini Agarwal, Girish Sastry, Amanda Askell, Pamela Mishkin, Jack Clark, et al. Learning transferable visual models from natural language supervision. In *International conference on machine learning*, pages 8748–8763. PMLR, 2021.

[45] Ahmed H Salamah, Kaixiang Zheng, Yiwen Liu, and En-Hui Yang. Jpeg inspired deep learning. *arXiv preprint arXiv:2410.07081*, 2024.

[46] Pouya Samangouei, Maya Kabkab, and Rama Chellappa. Defense-gan: Protecting classifiers against adversarial attacks using generative models. In *International Conference on Learning Representations*, 2018.

[47] Christian Schlarmann and Matthias Hein. On the adversarial robustness of multi-modal foundation models. In *Proceedings of the IEEE/CVF International Conference on Computer Vision*, pages 3677–3685, 2023.

[48] Christian Schlarmann, Naman Deep Singh, Francesco Croce, and Matthias Hein. Robust clip: Unsupervised adversarial fine-tuning of vision embeddings for robust large vision-language models. *arXiv preprint arXiv:2402.12336*, 2024.

[49] Changhao Shi, Chester Holtz, and Gal Mishne. Online adversarial purification based on self-supervision. *arXiv preprint arXiv:2101.09387*, 2021.

[50] Amanpreet Singh, Vivek Natarajan, Meet Shah, Yu Jiang, Xinlei Chen, Dhruv Batra, Devi Parikh, and Marcus Rohrbach. Towards vqa models that can read. In *Proceedings of the IEEE/CVF conference on computer vision and pattern recognition*, pages 8317–8326, 2019.

[51] Jiaming Song, Chenlin Meng, and Stefano Ermon. Denoising diffusion implicit models. *arXiv preprint arXiv:2010.02502*, 2020.

[52] Yang Song and Stefano Ermon. Generative modeling by estimating gradients of the data distribution. *Advances in neural information processing systems*, 32, 2019.

[53] Yang Song, Jascha Sohl-Dickstein, Diederik P Kingma, Abhishek Kumar, Stefano Ermon, and Ben Poole. Score-based generative modeling through stochastic differential equations. *arXiv preprint arXiv:2011.13456*, 2020.

[54] Florian Tramer, Nicholas Carlini, Wieland Brendel, and Aleksander Madry. On adaptive attacks to adversarial example defenses. *Advances in Neural Information Processing Systems*, 33, 2020.

[55] Ramakrishna Vedantam, C Lawrence Zitnick, and Devi Parikh. Cider: Consensus-based image description evaluation. In *Proceedings of the IEEE conference on computer vision and pattern recognition*, pages 4566–4575, 2015.

[56] Fenghua Weng, Yue Xu, Chengyan Fu, and Wenjie Wang. Mmj-bench: A comprehensive study on jailbreak attacks and defenses for vision language models. In *Proceedings of the AAAI Conference on Artificial Intelligence*, volume 39, pages 27689–27697, 2025.

[57] Eric Wong, Leslie Rice, and J Zico Kolter. Fast is better than free: Revisiting adversarial training. *arXiv preprint arXiv:2001.03994*, 2020.

[58] Xiyang Wu, Ruiqi Xian, Tianrui Guan, Jing Liang, Souradip Chakraborty, Fuxiao Liu, Brian M Sadler, Dinesh Manocha, and Amrit Bedi. On the safety concerns of deploying llms/vlms in robotics: Highlighting the risks and vulnerabilities. In *First Vision and Language for Autonomous Driving and Robotics Workshop*, 2024.

[59] Yongtao Wu, Fanghui Liu, Carl-Johann Simon-Gabriel, Grigoris Chrysos, and Volkan Cevher. Robust NAS under adversarial training: benchmark, theory, and beyond. In *The Twelfth International Conference on Learning Representations*, 2024.

[60] Ling Yang, Zhilong Zhang, Yang Song, Shenda Hong, Runsheng Xu, Yue Zhao, Wentao Zhang, Bin Cui, and Ming-Hsuan Yang. Diffusion models: A comprehensive survey of methods and applications. *ACM Computing Surveys*, 56(4):1–39, 2023.

[61] Jongmin Yoon, Sung Ju Hwang, and Juho Lee. Adversarial purification with score-based generative models. In *International Conference on Machine Learning*, pages 12062–12072. PMLR, 2021.

[62] Xiaohua Zhai, Basil Mustafa, Alexander Kolesnikov, and Lucas Beyer. Sigmoid loss for language image pre-training. In *Proceedings of the IEEE/CVF international conference on computer vision*, pages 11975–11986, 2023.

[63] Xiaohua Zhai, Xiao Wang, Basil Mustafa, Andreas Steiner, Daniel Keysers, Alexander Kolesnikov, and Lucas Beyer. Lit: Zero-shot transfer with locked-image text tuning. In *Proceedings of the IEEE/CVF conference on computer vision and pattern recognition*, pages 18123–18133, 2022.

[64] Jiaming Zhang, Qi Yi, and Jitao Sang. Towards adversarial attack on vision-language pre-training models. In *Proceedings of the 30th ACM International Conference on Multimedia*, pages 5005–5013, 2022.

- [65] Mingkun Zhang, Keping Bi, Wei Chen, Jiafeng Guo, and Xueqi Cheng. Clipure: Purification in latent space via clip for adversarially robust zero-shot classification. *arXiv preprint arXiv:2502.18176*, 2025.
- [66] Yi Zhang, Orestis Plevrakis, Simon S Du, Xingguo Li, Zhao Song, and Sanjeev Arora. Over-parameterized adversarial training: An analysis overcoming the curse of dimensionality. *Advances in Neural Information Processing Systems*, 33:679–688, 2020.
- [67] Yunqing Zhao, Tianyu Pang, Chao Du, Xiao Yang, Chongxuan Li, Ngai-Man Man Cheung, and Min Lin. On evaluating adversarial robustness of large vision-language models. *Advances in Neural Information Processing Systems*, 36:54111–54138, 2023.
- [68] Deyao Zhu, Jun Chen, Xiaoqian Shen, Xiang Li, and Mohamed Elhoseiny. Minigpt-4: Enhancing vision-language understanding with advanced large language models. *arXiv preprint arXiv:2304.10592*, 2023.

Contents of the Appendix

We organize the appendix as follows:

- In Appx. A, we provide complete proofs for Thm. 1 and 2 and Lemma 1.
- In Appx. B, we supply extend implementation details and ablation experiments, as well as the evaluation of DiffCAP under adaptive attacks. We further explore the potential of applying DiffCAP to other safety alignment challenges.
- In Appx. C, we discuss broader impact of this paper.

A Theoretical proofs

A.1 Proof of Thm. 1

Proof of Thm. 1. Expanding the forward diffusion solution from Eq. (5), we get:

$$\mathbf{x}(t) = \sqrt{\alpha(t)} \mathbf{x}_{\text{adv}} + \sqrt{1 - \alpha(t)} \boldsymbol{\epsilon} = \sqrt{\alpha(t)} \left[\mathbf{x} + \frac{\sqrt{1 - \alpha(t)}}{\sqrt{\alpha(t)}} \boldsymbol{\epsilon} + \boldsymbol{\epsilon}_{\text{adv}} \right], \quad \boldsymbol{\epsilon} \sim \mathcal{N}(0, I).$$

Given Asm. 1 and the property of Gaussian distribution, we can analyze the classifier output as follows by absorbing the scaling factor $\sqrt{\alpha(t)}$ and introduce $\boldsymbol{\epsilon}'$:

$$h(\mathbf{x}(t)) = h(\mathbf{x} + \boldsymbol{\epsilon}' + \boldsymbol{\epsilon}_{\text{adv}}), \quad \text{where } \boldsymbol{\epsilon}' \sim \mathcal{N}(0, \sigma(t)^2 I), \quad \sigma(t)^2 = \frac{1 - \alpha(t)}{\alpha(t)}.$$

Applying the randomized smoothing bound from Theorem 1 of [11], the classification is guaranteed to return class k_1 if:

$$\|\boldsymbol{\epsilon}_{\text{adv}}\|_2 < \frac{\sigma(t)}{2} (\Phi^{-1}(\underline{p}_1) - \Phi^{-1}(\overline{p}_2)).$$

By re-organizing the term, we get:

$$\sigma(t) > \frac{2\|\boldsymbol{\epsilon}_{\text{adv}}\|_2}{\Phi^{-1}(\underline{p}_1) - \Phi^{-1}(\overline{p}_2)}.$$

Since $\sigma(t)^2 = \frac{1 - \alpha(t)}{\alpha(t)}$, this yields:

$$\frac{1 - \alpha(t)}{\alpha(t)} > \left(\frac{2\|\boldsymbol{\epsilon}_{\text{adv}}\|_2}{\Phi^{-1}(\underline{p}_1) - \Phi^{-1}(\overline{p}_2)} \right)^2.$$

By re-organizing the term, we obtain:

$$\alpha(t) < \frac{1}{1 + \left(\frac{2\|\boldsymbol{\epsilon}_{\text{adv}}\|_2}{\Phi^{-1}(\underline{p}_1) - \Phi^{-1}(\overline{p}_2)} \right)^2}.$$

Since $\alpha(t) = \exp\left(-\int_0^t \beta(s) ds\right)$, and with linear schedule $\beta(t) = \beta_{\min} + (\beta_{\max} - \beta_{\min})t$, we compute:

$$\int_0^t \beta(s) ds = \beta_{\min} t + \frac{1}{2}(\beta_{\max} - \beta_{\min})t^2.$$

Thus,

$$\alpha(t) = \exp\left(-\beta_{\min} t - \frac{1}{2}(\beta_{\max} - \beta_{\min})t^2\right).$$

Let $M := \log\left(1 + \left(\frac{2\|\boldsymbol{\epsilon}_{\text{adv}}\|_2}{\Phi^{-1}(\underline{p}_1) - \Phi^{-1}(\overline{p}_2)}\right)^2\right)$. Then by setting:

$$\beta_{\min} t + \frac{1}{2}(\beta_{\max} - \beta_{\min})t^2 = M,$$

we obtain:

$$t = t_{\min} = \frac{2M}{\sqrt{\beta_{\min}^2 + 2(\beta_{\max} - \beta_{\min})M} + \beta_{\min}}.$$

Then, when $\beta_{\min} \geq M$, we have $t_{\min} \leq 1$, and for $t_{\min} \leq t \leq 1$, we have $\arg \max_{k \in [K]} \mathbb{P}(h(\mathbf{x}(t)) = k) = k_1$. \square

A.2 Proof of Lemma 1

Proof of Lemma 1. we have:

$$\mathbb{E} [\|\phi(\mathbf{x}(t_1)) - \phi(\mathbf{x}(t_2))\|_2] \leq L \cdot \mathbb{E} [\|\mathbf{x}(t_1) - \mathbf{x}(t_2)\|_2] \quad (8)$$

$$\leq L \cdot \sqrt{\mathbb{E} [\|\mathbf{x}(t_1) - \mathbf{x}(t_2)\|_2^2]}, \quad (9)$$

where Eq. (8) follows from the Lipschitz continuity of ϕ , Eq. (9) uses Jensen's inequality, i.e., $\mathbb{E}[\|Z\|] \leq \sqrt{\mathbb{E}[\|Z\|^2]}$ for any random vector Z .

Next, to compute $\mathbb{E} [\|\mathbf{x}(t_1) - \mathbf{x}(t_2)\|^2]$, use Eq. (5):

$$\mathbf{x}(t_1) - \mathbf{x}(t_2) = \left(\sqrt{\alpha(t_1)} - \sqrt{\alpha(t_2)} \right) \mathbf{x}_{\text{adv}} + \left(\sqrt{1 - \alpha(t_1)} - \sqrt{1 - \alpha(t_2)} \right) \boldsymbol{\epsilon},$$

where $\boldsymbol{\epsilon} \sim \mathcal{N}(0, I)$. Taking the squared norm and expectation:

$$\begin{aligned} \mathbb{E} [\|\mathbf{x}(t_1) - \mathbf{x}(t_2)\|^2] &= \left(\sqrt{\alpha(t_1)} - \sqrt{\alpha(t_2)} \right)^2 \|\mathbf{x}_{\text{adv}}\|^2 + \left(\sqrt{1 - \alpha(t_1)} - \sqrt{1 - \alpha(t_2)} \right)^2 \cdot \mathbb{E} [\|\boldsymbol{\epsilon}\|^2] \\ &= \left(\sqrt{\alpha(t_1)} - \sqrt{\alpha(t_2)} \right)^2 \|\mathbf{x}_{\text{adv}}\|^2 + \left(\sqrt{1 - \alpha(t_1)} - \sqrt{1 - \alpha(t_2)} \right)^2 d. \end{aligned}$$

As $t_1, t_2 \rightarrow 1$, both terms vanish, so the expectation tends to zero. \square

A.3 Proof of Thm. 2

Before proving Thm. 2, we need the following Lemma.

Lemma 2. Let $\beta(t) = \beta_{\min} + (\beta_{\max} - \beta_{\min})t$ be a linear noise schedule with $\beta_{\min} > 0$ and $\beta_{\max} > \beta_{\min}$. Define:

$$\alpha(t) := \exp \left(- \int_0^t \beta(s) \, ds \right), \quad \text{and} \quad f(t) := \beta(t) \cdot \sqrt{\frac{\alpha(t)}{1 - \alpha(t)}}.$$

Then $f(t)$ is strictly decreasing for all $t \in [0, 1]$.

Proof. We first analyze the function $f(t)$ by taking its logarithm:

$$\log f(t) = \log \beta(t) + \frac{1}{2} \log \left(\frac{\alpha(t)}{1 - \alpha(t)} \right).$$

Differentiating and using the chain rule, we get:

$$\begin{aligned} \frac{d}{dt} \log f(t) &= \frac{\beta'(t)}{\beta(t)} + \frac{1}{2} \left(\frac{d}{dt} \log \alpha(t) - \frac{d}{dt} \log(1 - \alpha(t)) \right) \\ &= \frac{\beta'(t)}{\beta(t)} + \frac{1}{2} \cdot \alpha'(t) \left(\frac{1}{\alpha(t)} + \frac{1}{1 - \alpha(t)} \right) \\ &= \frac{\beta'(t)}{\beta(t)} - \frac{1}{2} \cdot \frac{\beta(t)}{1 - \alpha(t)}, \end{aligned} \quad (10)$$

where we use $\alpha'(t) = -\beta(t) \cdot \alpha(t)$. Let's define $g(t) := \frac{d}{dt} \log f(t)$. We now analyze the sign of $g(t)$. First, observe that $\beta'(t) = \beta_{\max} - \beta_{\min} > 0$ is constant, $\beta(t) \geq \beta_{\min} > 0$, so $\frac{\beta'(t)}{\beta(t)}$ is strictly decreasing in t . Also $\alpha(t)$ is strictly decreasing, so $1 - \alpha(t)$ is strictly increasing, and hence $\frac{\beta(t)}{1 - \alpha(t)}$ is

strictly increasing. Therefore, $g(t)$ is strictly decreasing in t . To show that $g(t) < 0$ for all $t \in [0, 1]$, it suffices to show $g(t) < 0$ near $t = 0$.

When $t \approx 0$, we have:

$$\beta(t) \approx \beta_{\min}, \quad \int_0^t \beta(s) ds \approx \beta_{\min} t, \quad \alpha(t) = \exp(-\beta_{\min} t) \approx 1 - \beta_{\min} t + o(t).$$

Thus,

$$\frac{\beta(t)}{1 - \alpha(t)} \approx \frac{\beta_{\min}}{\beta_{\min} t} = \frac{1}{t}, \quad \text{which diverges as } t \rightarrow 0.$$

Given the result:

$$\frac{\beta'(t)}{\beta(t)} \approx \frac{\beta_{\max} - \beta_{\min}}{\beta_{\min}},$$

which is a finite number, thus, $g(t) \rightarrow -\infty$ as $t \rightarrow 0$. Since $g(t)$ is strictly decreasing, it follows that $g(t) < 0$ for all $t \in [0, 1]$. This implies that $\log f(t)$ is strictly decreasing, and thus $f(t)$ is strictly decreasing as well. \square

Now we are ready to present the proof of Thm. 2.

Proof of Thm. 2. Let $\Delta(t, \delta) := \mathbf{x}(t + \delta) - \mathbf{x}(t)$. From the closed-form solution of the VP-SDE,

$$\mathbf{x}(t) = \sqrt{\alpha(t)} \mathbf{x}_{\text{adv}} + \sqrt{1 - \alpha(t)} \boldsymbol{\epsilon}_{\text{adv}},$$

we have:

$$\Delta(t, \delta) = \left(\sqrt{\alpha(t + \delta)} - \sqrt{\alpha(t)} \right) \mathbf{x}_{\text{adv}} + \left(\sqrt{1 - \alpha(t + \delta)} - \sqrt{1 - \alpha(t)} \right) \boldsymbol{\epsilon}_{\text{adv}}.$$

Let us define:

$$A := \sqrt{\alpha(t + \delta)} - \sqrt{\alpha(t)}, \quad B := \sqrt{1 - \alpha(t + \delta)} - \sqrt{1 - \alpha(t)}. \quad (11)$$

Then: $\Delta(t, \delta) = A \mathbf{x}_{\text{adv}} + B \boldsymbol{\epsilon}$. By the Lipschitz property of ϕ and the Cauchy-Schwarz inequality:

$$\mathbb{E} [\|\phi(\mathbf{x}(t + \delta)) - \phi(\mathbf{x}(t))\|_2] \leq L \cdot \mathbb{E} [\|\Delta(t, \delta)\|_2] \leq L \cdot \sqrt{\mathbb{E} [\|\Delta(t, \delta)\|_2^2]}, \quad (12)$$

where $L \in \{L_1, L_2\}$. We now compute this second moment:

$$\mathbb{E} [\|\Delta(t, \delta)\|_2^2] = \mathbb{E} [\|A \mathbf{x}_{\text{adv}} + B \boldsymbol{\epsilon}\|_2^2] = A^2 \|\mathbf{x}_{\text{adv}}\|_2^2 + B^2 \mathbb{E} [\|\boldsymbol{\epsilon}\|_2^2].$$

Since $\boldsymbol{\epsilon}$ is standard Gaussian in \mathbb{R}^d , we get: $\mathbb{E} [\|\boldsymbol{\epsilon}\|_2^2] = d$. Thus:

$$\mathbb{E} [\|\Delta(t, \delta)\|_2^2] = A^2 \|\mathbf{x}_{\text{adv}}\|_2^2 + B^2 d.$$

We now perform Taylor expansion for A and B with respect to t . First note that:

$$\frac{d}{dt} \alpha(t) = -\beta(t) \alpha(t), \quad \frac{d}{dt} \sqrt{\alpha(t)} = -\frac{\beta(t)}{2} \sqrt{\alpha(t)}.$$

Plugging the above equation back into Eq. (11), we get:

$$A = \sqrt{\alpha(t + \delta)} - \sqrt{\alpha(t)} = -\frac{\beta(t)}{2} \sqrt{\alpha(t)} \delta + o(\delta).$$

Similarly:

$$\frac{d}{dt} \sqrt{1 - \alpha(t)} = \frac{\beta(t) \alpha(t)}{2 \sqrt{1 - \alpha(t)}}.$$

Plugging the above equation back into Eq. (11), we get:

$$B = \sqrt{1 - \alpha(t + \delta)} - \sqrt{1 - \alpha(t)} = \frac{\beta(t) \alpha(t)}{2 \sqrt{1 - \alpha(t)}} \delta + o(\delta).$$

Table 5: Evaluation of OpenFlamingo (OF-9B) and LLaVA 1.5-7B on four datasets under clean and adversarial ($\ell_\infty^{8/255}$) conditions, with and without DiffCAP defense against adaptive attacks.

VLM	Dataset	Clean		APGD		BPDA		BPDA + EOT	
		w/o	with	w/o	with	w/o	with	w/o	with
OF [6]	COCO [31]	90.1	92.4	4.7	91.1	27.1	79.9	29.2	83.4
	Flicker30k [42]	63.9	62.7	4.9	60.5	19.1	50.6	15.5	56.5
	TextVQA [50]	23.1	18.6	0.6	17.6	7.1	18.2	2.3	16.0
	VQAv2 [18]	46.2	47.1	8.3	44.6	24.0	44.5	18.0	39.5
LLaVA [33]	COCO [31]	125.9	122.2	11.3	123.4	21.9	115.9	19.5	114.9
	Flicker30k [42]	81.7	78.0	8.5	76.2	20.9	73.4	18.0	74.6
	TextVQA [50]	36.9	25.1	7.4	22.7	8.8	24.3	8.7	21.7
	VQAv2 [18]	74.3	69.9	23.4	67.5	25.7	65.4	27.1	66.9

Take the square and sum them up, we obtain:

$$A^2 + B^2 = \frac{\beta(t)^2 \delta^2}{4} \left(\alpha(t) + \frac{\alpha(t)^2}{1 - \alpha(t)} \right) + o(\delta^2) = \frac{\beta(t)^2 \alpha(t) \delta^2}{4(1 - \alpha(t))} + o(\delta^2).$$

Since $\|\mathbf{x}_{\text{adv}}\|^2 \leq d$, we have:

$$\mathbb{E} [\|\Delta(t, \delta)\|_2^2] \leq \frac{d \cdot \beta(t)^2 \alpha(t)}{4(1 - \alpha(t))} \delta^2 + o(\delta^2). \quad (13)$$

Plugging Eq. (13) into Eq. (12), we obtain:

$$\mathbb{E} [\|\phi(\mathbf{x}(t + \delta)) - \phi(\mathbf{x}(t))\|_2] \leq L \cdot \sqrt{\mathbb{E} [\|\Delta(t, \delta)\|_2^2]} = O \left(L \delta \cdot \beta(t) \sqrt{\frac{\alpha(t)}{1 - \alpha(t)}} \right).$$

Lastly, by Lemma 2, we have that the bound on the right hand side decreases as t grows. \square

B Additional experiment

B.1 More implementation details

For the forward diffusion, we schedule noise with $\beta_{\min} = 0.1$, $\beta_{\max} = 20$, and a fixed step size of 0.01. In the reverse generation, we employ guided diffusion with a step size of 0.015. To keep the evaluation of adaptive attacks on large vision-language models (VLMs) computationally tractable, we randomly choose 100 images per dataset. BPDA [4] attacks are run for 50 iterations, while EOT [5] attacks are approximated using three stochastic samples per query. For stronger attacks with $\epsilon > 4/255$, we set the minimum diffusion depth to 0.04 for sufficient denoising. All baseline methods are evaluated using their respective best-performing hyperparameters as reported in the original papers.

B.2 Adaptive attacks

We evaluate DiffCAP in a *white-box* setting, where the adversary has full knowledge of the deployed defense mechanism. Tab. 5 presents the detailed metrics for image captioning (IC) and visual-question answering (VQA) tasks across various attack configurations, comparing performance with and without DiffCAP defense. Even under an increased attack budget ($\ell_\infty^{8/255}$), DiffCAP maintains high fidelity on clean inputs, with only an average performance drop of 3.3 points. Under APGD [12] attacks, when the adversary is unaware of DiffCAP's existence, it successfully restores the performance of VLMs on different datasets to levels closely matching their clean baselines, showing only a modest average degradation of 4.8 points.

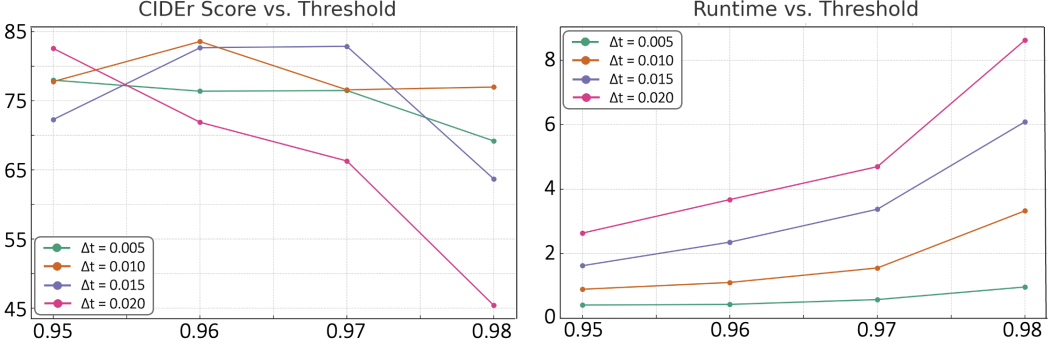


Figure 4: CIDEr score and running time (in second) per image with varying thresholds and diffusion step sizes (Δt) for DiffCAP. The evaluation is based on the image captioning task under $\ell_\infty^{2/255}$ attack.

Table 6: Evaluation of DiffCAP in mitigating Hallucination and Jailbreaking of large VLMs.

	Hallucination with LLaVA 1.5-13B			Jailbreaking with MiniGPT 4-13B				
	adversarial	popular	random	any	identity	disinfo	crime	x-risk
Clean	82.7	84.3	85.0	16/40	3/11	6/13	6/13	1/3
Attack	N/A	N/A	N/A	24/40	6/11	7/13	12/13	2/3
DiffCAP	83.2	85.1	86.3	14/40	3/11	5/13	5/13	1/3

In scenarios where the adversary bypasses gradient obfuscation through backward pass differentiable approximation (BPDA) [4] and simulates stochasticity via expectation over transformations (EOT) [5], DiffCAP continues to demonstrate strong resilience. The best-case performance degradation relative to clean conditions is only 1.7 points (OF-VQAv2) by BPDA without EOT and 6.7 points (OF-COCO) with EOT. The corresponding worst-case performance reductions are observed as 13.3 points (OF-Flickr30k) and 15.2 points (LLaVA-TextVQA), respectively. These results elucidate the inherent uncertainty of DiffCAP’s per-image diffusion step calculation, which determines the minimal purification for each adversarial example based on semantic convergence during the diffusion process. Such a dynamic strategy significantly prevents trivial gradient approximations and random regressions from circumventing its defense, enhancing adversarial robustness against adaptive attacks of prohibitively high time complexity.

B.3 Ablation on threshold and diffusion step size

To validate the effectiveness of the adaptive similarity threshold calculation described in Alg. 2, we conduct an ablation study over different threshold values τ and diffusion step sizes Δt . Fig. 4 displays the results by OF on the COCO dataset. We observe that setting the threshold to 0.96 achieves the best overall robustness in terms of CIDEr score across a range of step sizes. A higher threshold generally leads to more diffusion steps, increasing time for reverse diffusion sampling. In practice, we find that a step size of 0.01 offers the best trade-off between performance and computational cost. Notably, $\tau = 0.96$ and $\Delta t = 0.01$ used in our main experiments bring about an average overhead of 1.1 seconds per image, significantly faster than ~ 2.3 seconds per image required by DiffPure.

B.4 Hallucination and jailbreaking

Large VLMs tend to hallucinate objects that are not actually present in the image. POPE [30] serves as a benchmark to formulate hallucination detection as a binary classification task. In Tab. 6, we report the F1-scores across three POPE categories using LLaVA 1.5-13B, with and without DiffCAP applied as image preprocessing. A consistent improvement is observed with DiffCAP. This suggests that DiffCAP, through Langevin dynamics, walks image features to semantically stable regions of the distribution. By suppressing high-frequency adversarial or spurious signals, DiffCAP becomes less sensitive to misleading cues and more robust against hallucination.

Large VLMs are also vulnerable to jailbreaking attacks on the visual modality [7, 43], where adversarially crafted images can induce harmful outputs in response to restricted prompts (e.g., “*How to make a bomb?*”). We apply the attack proposed by Qi et al. [43] to MiniGPT 4-13B [68] and count the policy-violating outputs triggered by 40 harmful prompts spanning four categories. Even under a stronger perturbation budget ($\ell_{\infty}^{16/255}$), DiffCAP successfully restores the model’s behavior to a level comparable to, or slightly better than, the clean condition. These findings reinforce the versatility of DiffCAP as a modular defense measure, readily adaptable to various models and tasks requiring robustness guarantee. As jailbreaking attacks continue to evolve rapidly, benchmarking DiffCAP against such threats falls outside the scope of this work, but nonetheless marks a promising direction for future investigation.

C Broader impact

With the swift application of VLMs, the risk of adversarial attacks has become a critical concern. This paper proposes DiffCAP, an adversarial purification method that can improve robustness without retraining the model, which may enlarge its usability in application scenarios, such as autonomous driving based on VLMs. While maintaining a remarkable defense effect, this method greatly reduces the diffusion steps and hyperparameter adjustments, which promotes the safe and fast implementation for defending pre-trained large models. However, any single defense mechanism may fail in face of new attacks, so maintaining a diverse and regularly tested defense strategy is essential.